Asian Journal of Pharmaceutical Sciences 20 (2025) 101006

Available online at www.sciencedirect.com

ScienceDirect

journal homepage: www.elsevier.com/locate/AJPS

Research Article

Exosome-membrane and polymer-based hybrid-complex for systemic delivery of plasmid DNA into brains for the treatment of glioblastoma

Youngki Lee[a], *Subin Kang*[a], *Le Thi Thuy*[b], *Mincheol Son*[a], *Jae Young Park*[a], *Sung Bin Ahn*[a], *Minji Kang*[a], *Jihun Oh*[a], *Joon Sig Choi*[b,*], *Minhyung Lee*[a,*]

[a] *Department of Bioengineering, Hanyang University, Seoul, 04763, Republic of Korea*
[b] *Department of Biochemistry, Chungnam National University, Daejeon, 34134, Republic of Korea*

ARTICLE INFO

Article history:
Received 18 April 2024
Revised 2 October 2024
Accepted 12 October 2024
Available online 12 December 2024

Keywords:
Exosome
Glioblastoma
Plasmid DNA
Polymeric carrier
Targeted delivery

ABSTRACT

Herpes simplex virus thymidine kinase (HSVtk) gene therapy is a promising strategy for glioblastoma therapy. However, delivery of plasmid DNA (pDNA) encoding HSVtk into the brain by systemic administration is a challenge since pDNA can hardly penetrate the blood-brain barrier. In this study, an exosome-membrane (EM) and polymer-based hybrid complex was developed for systemic delivery of pDNA into the brain. Histidine/arginine-linked polyamidoamine (PHR) was used as a carrier. PHR binds to pDNA by electrostatic interaction. The pDNA/PHR complex was mixed with EM and subjected to extrusion to produce pDNA/PHR-EM hybrid complex. For glioblastoma targeting, T7 peptide was attached to the pDNA/PHR-EM complex. Both pDNA/PHR-EM and T7-decorated pDNA/PHR-EM (pDNA/PHR-EM-T7) had a surface charge of –5 mV and a size of 280 nm. Transfection assays indicated that pDNA/PHR-EM-T7 enhanced the transfection to C6 cells compared with pDNA/PHR-EM. Intravenous administration of pHSVtk/PHR-EM-T7 showed that pHSVtk/PHR-EM and pHSVtk/PHR-EM-T7 delivered pHSVtk more efficiently than pHSVtk/lipofectamine and pHSVtk/PHR into glioblastoma *in vivo*. pHSVtk/PHR-EM-T7 had higher delivery efficiency than pHSVtk/PHR-EM. As a result, the HSVtk expression and apoptosis levels in the tumors of the pHSVtk/PHR-EM-T7 group were higher than those of the other control groups. Therefore, the pDNA/PHR-EM-T7 hybrid complex is a useful carrier for systemic delivery of pHSVtk to glioblastoma.

* Correspoding authors at: Department of Bioengineering, Hanyang University, Seoul 04763 and Department of Biochemistry, Chungnam National University, Daejeon, 34134, Republic of Korea.
E-mail addresses: joonsig@cnu.ac.kr (J.S. Choi), minhyung@hanyang.ac.kr (M. Lee).
Peer review under responsibility of Shenyang Pharmaceutical University.

https://doi.org/10.1016/j.ajps.2024.101006

1. Introduction

Glioblastoma is a grade IV brain tumor with a high mortality rate [1]. Therapeutic options for glioblastoma include conventional clinical therapies such as surgical resection, chemical therapy, and radiotherapy [2]. However, these therapeutic options have limitations in improving patient outcomes, since recurrence after conventional therapies is common in glioblastoma patients [3]. Therefore, the prognosis for glioblastoma patients remains poor, with a short life span less than two years. Thus, new therapeutic modalities have been investigated to improve therapeutic outcomes in glioblastoma treatments.

As a new therapeutic modality, gene therapy has been studied for glioblastoma therapy. Successful delivery of therapeutic genes may inhibit tumor cell proliferation and induce cell death in the tumors. Two requirements should be satisfied for gene therapy. First, therapeutic genes should induce effective tumor growth inhibition and cell death. Various therapeutic genes have been investigated as therapeutic genes for glioblastoma, including toxin and suicide genes [4,5]. The most widely investigated therapeutic gene for glioblastoma in many preclinical and clinical tests is the herpes simplex virus type 1 thymidine kinase (HSVtk) gene [6,7]. In cells, HSVtk can convert a prodrug, ganciclovir (GCV), into an anti-cancer drug, triggering cell death [8]. In addition, a toxic anti-cancer drug produced by HSVtk can be transported to neighboring tumor cells through a gap-junction. This effect of HSVtk is called the 'bystander effect' and leads to effective glioblastoma therapy [9].

Another important factor for successful gene therapy is the carrier of therapeutic genes. Despite the effect of therapeutic genes, gene delivery into the brain is a major challenge. The delivery of genes into the brain is inefficient due to the blood-brain-barrier (BBB), which is a selective barrier that regulates the entry of substances into the brain. Most drugs and therapeutics cannot effectively penetrate the BBB [10]. Therefore, a gene delivery platform that can penetrate the BBB is required for successful gene therapy of glioblastoma. Recently, exosomes have been suggested as an efficient carrier of various drugs, including therapeutic nucleic acids into the brains [11–19]. Small therapeutic nucleic acids such as small interfering RNAs (siRNAs) were delivered into the brains using exosomes by systemic administration [15,20]. The results indicated that exosomes were an efficient carrier for siRNAs or therapeutic oligonucleotides into the brain. However, the size of the nucleic acids is an important factor that determines the loading efficiency and loading large therapeutic gene such as plasmid DNA (pDNA) and messenger RNA (mRNA) is significantly challenging. Compared to small nucleic acids, larger therapeutic acids do not diffuse well into exosomes due to the higher repulsive negative charge of the phosphate backbone [21]. Moreover, the exogenous loading method is inefficient and problematic, further hindering the encapsulation process. In general, loading of nucleic acids into the exosomes has been performed by electroporation, sonoporation, or freeze-thaw methods. Electroporation has been widely used [11,12,22], but its the loading efficiency was only 2% [12,23]. During electroporation, electric pulses create temporary pores in the exosome membranes, through which therapeutic nucleic acids can passively diffuse. Therefore, the concentration of nucleic acids in exosomes cannot exceed that of the outside environment. In previous studies, pDNAs were transfected into cells for passive loading during exosome production. However, the loading efficiency of pDNA into exosomes was lower than that of small nucleic acids due to the larger size [24,25].

In a previous study, cell-membrane-coated DNA nanoparticles were investigated as a gene carrier for local injection into the brain [7]. To produce DNA nanoparticles, pDNA was condensed with polymeric carriers. Cationic polymers such as polyethylenimine (PEI), chitosan, or polyamidoamine (PAMAM) dendrimer were used to condense pDNA into nanoparticles [26–28]. Then, the cell membrane was mixed with the condensed DNA nanoparticles and subjected to extrusion. Cell-membrane-coated DNA nanoparticles were injected locally into the brain for gene delivery into the glioblastoma [7]. Cell-membrane-coated DNA nanoparticles effectively delivered pDNA into the glioblastoma cells and produced therapeutic effects. However, systemic delivery of pDNA into the brain using cell-membrane-coated DNA nanoparticles has not been investigated.

In a previous study, PAMAM conjugated with histidine and arginine (PHR) was used as a pDNA carrier into the brain [29]. Due to the positive charge of arginine and histidine residues, PHR can bind to the negatively charged phosphate backbone of nucleic acids through electrostatic interaction. Local injection into the brain showed that the pDNA/PHR complex delivered pDNA more efficiently than the pDNA/PEI complex. Additionally, PHR demonstrated advantages in terms of cytotoxicity, serum tolerance, and endosomal escape. However, PHR may not be suitable for systemic delivery. Firstly, pDNA/PHR should be delivered into the brain through BBB. However, pDNA/PHR did not contain targeting ligands for delivery into the brain. Secondly, the pDNA/PHR complexes have high positive surface charge, which may induce opsonization in blood, resulting in rapid clearance of the complexes [30]. Therefore, surface modification of the pDNA/PHR complex may be required for systemic application of PHR as a gene carrier. As described above, exosomes are an efficient carrier of various drugs including small nucleic acids for systemic administration. Exosomes penetrated the BBB efficiently for delivery of therapeutic agents into the brain. According to this observation, we hypothesized that pDNA, exosome-membrane (EM), and PHR hybrid-complex might increase circulation time and delivery efficiency into the brain. In the current study, EM from C6 glioblastoma cells was used to prepare the pHSVtk/PHR-EM hybrid-complex. In addition, pHSVtk/PHR-EM was decorated with T7 peptide (HAIYPRH) for brain targeting delivery. T7 peptides are a ligand for transferrin receptors, and the binding of T7 peptide to its receptors enhanced transcytosis of the complexes into the brain [31]. Therefore, cholesterol-linked T7 peptide (T7c) was mixed with pHSVtk/PHR-EM to produce T7-decorated pHSVtk/PHR-EM (pHSVtk/PHR-EM-T7). pHSVtk/PHR-EM and pHSVtk/PHR-EM-T7 were evaluated in an orthotopic glioblastoma model in terms of delivery efficiency and therapeutic efficacy.

2. Materials and methods

2.1. Materials

The C6 rat glioblastoma cell line was supplied by the Korean Cell Line Bank (Seoul, Korea). Dulbecco's Modified Eagle Medium (DMEM), Dulbecco's phosphate-buffered saline (DPBS), and exosome-depleted fetal bovine serum (FBS) were acquired from Welgene (Seoul, Korea). Plasmid Maxiprep Kit and exoEasy Maxi kit were acquired from Qiagen (Valencia, CA). Cholesterol-linked T7 (cholesterol-HAIYPRH, T7c) was synthesized by Peptron (Daejeon, Korea). Extruder and membranes were acquired from Avanti (Birmingham, AL). Luciferase substrate (luciferin) and lysis buffer were acquired from Promega (Madison, WI). The bicinchoninic acid (BCA) protein assay and lipofectamine were acquired from Thermo Scientific (Rockford, IL). A nucleic acid-labeling kit was acquired form Mirus-Bio (Madison, WI). Cy5.5 NHS ester, Terminal deoxynucleotidyl transferase dUTP nick end labeling (TUNEL) kit, and anti-thymidine kinase rabbit monoclonal antibody were acquired from Abcam (Waltham, MA). GCV was obtained from Invivogen (San Diego, CA). pHSVtk and pLuc were constructed previously [32].

2.2. Preparation of pHSVtk/PHR-EM and pHSVtk/PHR-EM-T7

C6 cells were maintained in DMEM containing 10% FBS for 72 h Exosomes were separated from the culture medium using the ExoEasy Maxi kit. The isolated exosomes were lysed by ultrasonication for 3 min. Protein concentration in EM was measured with the BCA assay kit. Synthesis of PHR was performed as described as described previously [29]. Synthesis scheme was presented in Supplementary Fig. S. The synthesis of PHR was confirmed by ^{1}H NMR (Fig. S2).

For preparation of the pHSVtk/PHR complexes, PHR was mixed with pHSVtk at different weight ratios in 5% glucose solution. For complex formation, the samples were kept at room temperature for 30 min. For preparation of pHSVtk/PHR-EM, the pHSVtk/PHR complex was prepared at a 1:12 wt ratio. Then, EM were mixed with pHSVtk/PHR at various ratios. The mixtures were subjected to 10 rounds of extrusion through 0.1-μm polycarbonate membranes. Decoration of the pHSVtk/PHR-EM complex with T7 peptide was performed by addition of T7c to pHSVtk/PHR-EM at various weight ratios. Then, the mixtures were subjected to extrusion for another 10 cycles.

To evaluate the integration level of T7c to pHSVtk/PHR-EM, the mixture of pHSVtk/PHR-EM and Flamma 648-labeled T7c (F648-T7c) were centrifuged at 13,000× *g* for 30 min to precipitate pHSVtk/PHR-EM-T7. F648-T7c solution was centrifuged as a control. After centrifugation, the supernatant of the sample and control was harvested, and the fluorescence level was measured by a fluorometer at 648 nm/663 nm. The T7c integration rate to pHSVtk/PHR-EM was calculated as follows:

$$\text{T7c integration rate (\%)} = [1 - \text{Fluorescence of the supernatant(sample)}/\text{Fluorescence of the supernatant (control)}] \times 100\%$$

2.3. Transfection assay

C6 cells were inoculated on 12-well plates at 1×10^5 cells/well and were cultured at 37 °C for 24 h Prior to transfection, the cell-culture media were replaced with fresh DMEM containing 10% FBS. For the endosomal escape study, chloroquine was added at 30 min before transfection at a concentration of 60 μM. pLuc/PHR, pLuc/PHR-EM, and pLuc/PHR-EM-T7 were prepared as described above and added to the cells. The complexes were incubated with the cells for 4 h Then, the media were replaced with fresh DMEM containing 10% FBS. The cells were cultured for an additional 24 h Luciferase assay was performed as described previously [7,33].

2.4. Dynamic light scattering and TEM

pHSVtk/PHR, pHSVtk/PHR-EM, and pHSVtk/PHR-EM-T7 were prepared, and their zeta potentials and sizes were measured with a Zetasizer (Malvern Instruments, Malvern, UK). The samples were prepared on mesh copper grids (Ted Pell, Redding, CA) as described previously [34]. The samples were analyzed using transmission electron microscopy (TEM; JEOL, Tokyo, Japan).

2.5. Flow cytometry

pHSVtk was labeled with Cy5 using a labeling kit. To evaluate the cellular uptake pathway, the cells were treated with various inhibitors at 30 min before transfection (10 μM chlorpromazine, 0.4 μg/ml filipin III, 200 μM amiloride, and 1.5 mM methyl-β-cyclodextrin), according to the previous study [28,29]. Transfection was performed at a concentration of 0.2 μg pHSVtk/well. Flow cytometry was performed as described previously [35,36].

2.6. Confocal microscopy and hemocompatibility assay

C6 cells were plated on a chamber slide at 1×10^5 cells/well. Cy5- pHSVtk/PHR, Cy5-pHSVtk/PHR-EM, and Cy5-pHSVtk/PHR-EM-T7 were transfected into the cells. Then, the slides were washed with DPBS and fixed with 4% paraformaldehyde. DAPI was used to counterstain the nuclei. The slides were observed using confocal microscopy (Leica Microsystems, Wetzlar, Germany) as described previously [37]. Hemocompatibility assay was performed with erythrocytes as described previously [15].

2.7. Transcytosis study

The *in vitro* transwell model assay was performed to evaluate PHR-EM-T7 transcytosis. The transwell assay was performed as described previously [15]. The bEND.3 mouse endothelial cells were cultured in a transwell plate and C6 cells were cultured in a bottom well. Cy5-pHSVtk/PHR-EM or Cy5-pHSVtk/PHR-EM-T7 were added into the transwell. After 24 h of incubation, bEND.3 and C6 cells on the basolateral side were harvested. Relative cellular uptake of Cy5-pHSVtk was measured from bEND.3 and C6 cells by flow cytometry.

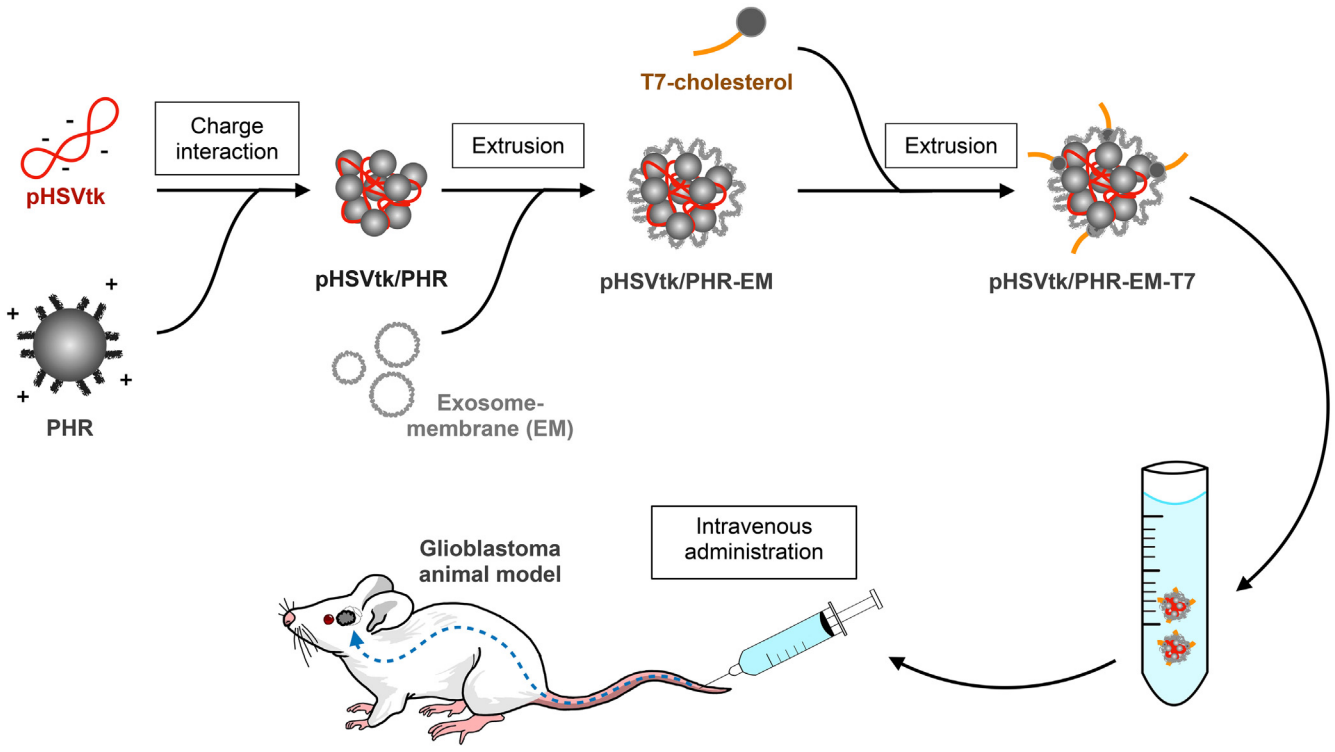

Fig. 1 – Schematic representation of preparation of the pDNA/PHR-EM-T7 hybrid-complex.

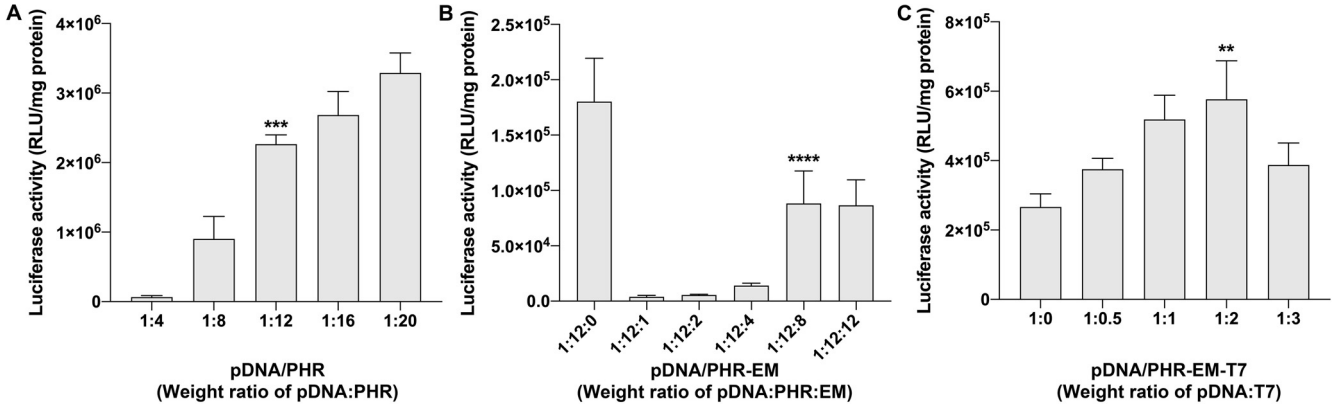

Fig. 2 – Optimization of the complex weight ratios for transfection. The pLuc/PHR (A), pLuc/PHR-EM (B), and pLuc/PHR-EM-T7 (C) complexes were transfected to C6 cells at different weight ratios. The transfection efficiency was measured by luciferase assay ($n = 4$). **$P < 0.01$ compared with 1:0, 1:0.5 and 1:3,*$P < 0.001$ compared with 1:4, 1:8 and 1:20, ****$P < 0.0001$ compared with 1:12:0, 1:12:1, 1:12:2 and 1:12:4. (For interpretation of the references to colour in this figure legend, the reader is referred to the web version of this article.)**

2.8. *Orthotopic rat glioblastoma model*

All experimental animal protocols were approved by the Institutional Animal Care and Use Committee (IACUC) at Hanyang University (accreditation number: 2020–0238A). The orthotopic glioblastoma model was produced by transplant of C6 cells by stereotaxic injection into seven-week-old male SD rats as described previously [38]. After one week, complexes were injected intravenously at a dose of 30 μg of pHSVtk in 1 ml DPBS. GCV was injected intraperitoneally at a dose of 30 mg/kg every 24 h After one week, the rats were sacrificed. The brains were harvested, fixed with 4% paraformaldehyde, and embedded in paraffin.

2.9. *Biodistribution*

Naked Cy5.5-pHSVtk, Cy5.5-pHSVtk/lipofectamine, Cy5.5-pHSVtk/PHR, Cy5.5-pHSVtk/PHR-EM, and Cy5.5-pHSVtk/PHR-EM-T7 were prepared at their optimal ratios. The complexes were injected intravenously into the orthotopic glioblastoma

animal model at 30 μg Cy5.5-pHSVtk per rat. After 2 h, *ex vivo* fluorescence images were obtained using a Fluorescence In Vivo Imaging System (FOBI system, Neo Science, Suwon, Korea).

2.10. *H&E, immunofluorescence and NISSL staining*

The tissues were fixed, embedded in paraffin, and cut into 5-μm-thick sections. The sections were deparaffinized, rehydratedand stained with Hematoxylin and eosin (H&E). The paraffin-embedded brain tissues were sliced into 5-μm-thick sections. Immunofluorescence staining was performed with anti-thymidine kinase antibody and TUNEL assay kit as described previously [39,40]. The 5-μm-thick brain sections were stained with 0.1% cresyl violet, and tumor size was measured with ImageJ software.

2.11. *Statistical analysis*

Data are presented as mean ± standard deviation (SD). Differences among groups were determined by analysis of variance followed by a Newman–Keuls test. *P* values less than 0.05 were considered statistically significant.

3. Results and discussion

3.1. *Characterization of pDNA/PHR-EM and pDNA/PHR-EM-T7*

Exosomes are a promising carrier of therapeutic nucleic acids into the brain by systemic administration. However, loading of pDNA into exosomes is inefficient due to its larger size. To apply the advantages of exosomes for pDNA delivery into the brain, a hybrid system with EM and PHR was developed, producing pDNA/PHR-EM-T7. The pDNA/PHR complexes were mixed with EM and subjected to extrusion (Fig. 1). Then, the targeting ligand, T7c, was attached to pDNA/PHR-EM by hydrophobic interactions with EM (Fig. 1). T7 is a specific ligand to the transferrin receptor, with which binding on the surface of pDNA/PHR-EM-T7 may facilitate the transcytosis of the complex into the brain tissue across the BBB [31].

The optimal ratio of pDNA, PHR, EM, and T7 was determined by *in vitro* transfection assay with pLuc. First, the optimal ratio between pLuc and PHR was determined by transfection assay. pLuc/PHR at different weight ratios was transfected into C6 cells. The results showed increased efficiency along with increasing ratio of PHR, which began to plateau around a 1:12 (wt) (Fig. 2A). Although the transfection efficiency at a 1:16 ratio was higher than that at a 1:12 ratio, the difference was not statistically significant. This result is coincident with a previous report [29]. According to this result, the weight ratio between pLuc and PHR was fixed at 1:12 for the following experiments.

The pLuc/PHR-EM hybrid-complex was prepared by mixing various amounts of EM to pDNA/PHR. The transfection assay with pLuc/PHR-EM indicated the highest transfection efficiency at a 1:12:8 ratio of pDNA:PHR:EM (Fig. 2B). However, the transfection efficiency of the hybrid-complex was lower than that of pLuc/PHR. This may be due to the negative surface

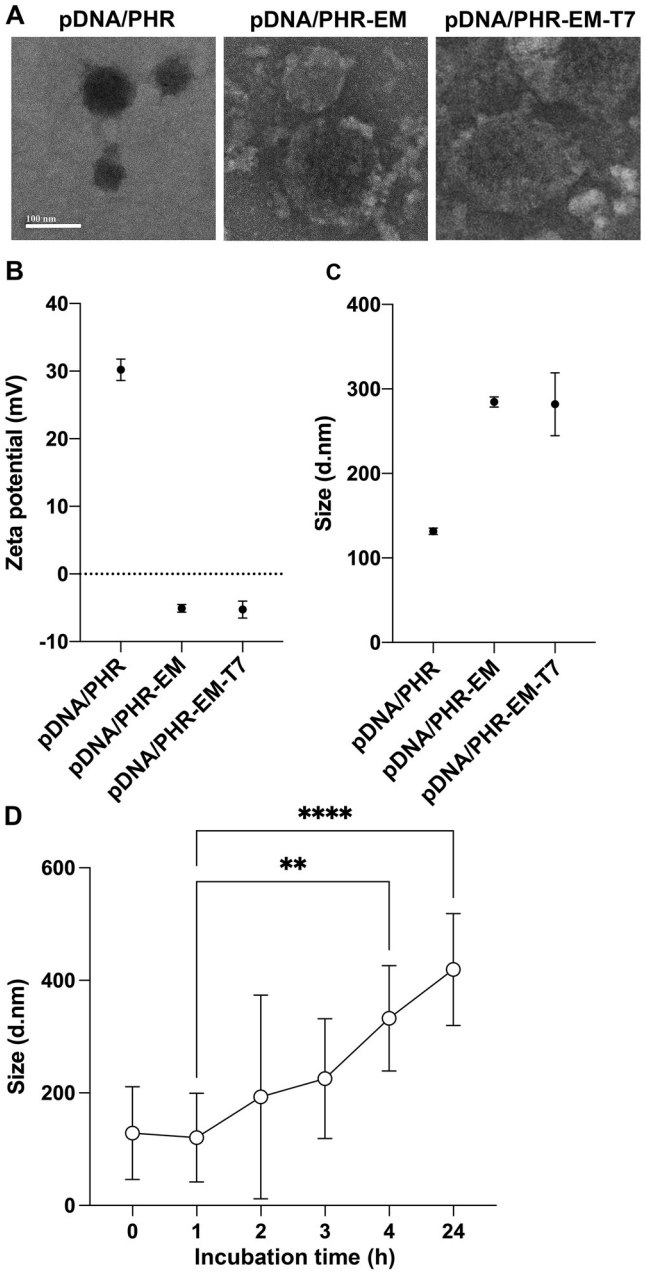

Fig. 3 – Physical characterization of the complex. The complexes were analyzed using TEM (A), zeta potential (B) and complex size (C). The scale bar is 100 nm. Time-dependent size changes (D) were measured at various time points. **P < 0.01, ****P < 0.0001. (For interpretation of the references to colour in this figure legend, the reader is referred to the web version of this article.)

charge of pLuc/PHR-EM, which may reduce the interactions with cell membranes. The transfection efficiency of pLuc/PHR-EM reached its plateau at a 1:12:8 (wt). This tendency was similar to the results with cell-membrane-coated DNA nanoparticles in a previous study [7].

For targeted pDNA delivery to glioblastoma, T7 peptide was attached to the surface of the pDNA/PHR-EM complex. To enable the T7 peptide to embed in the membrane through

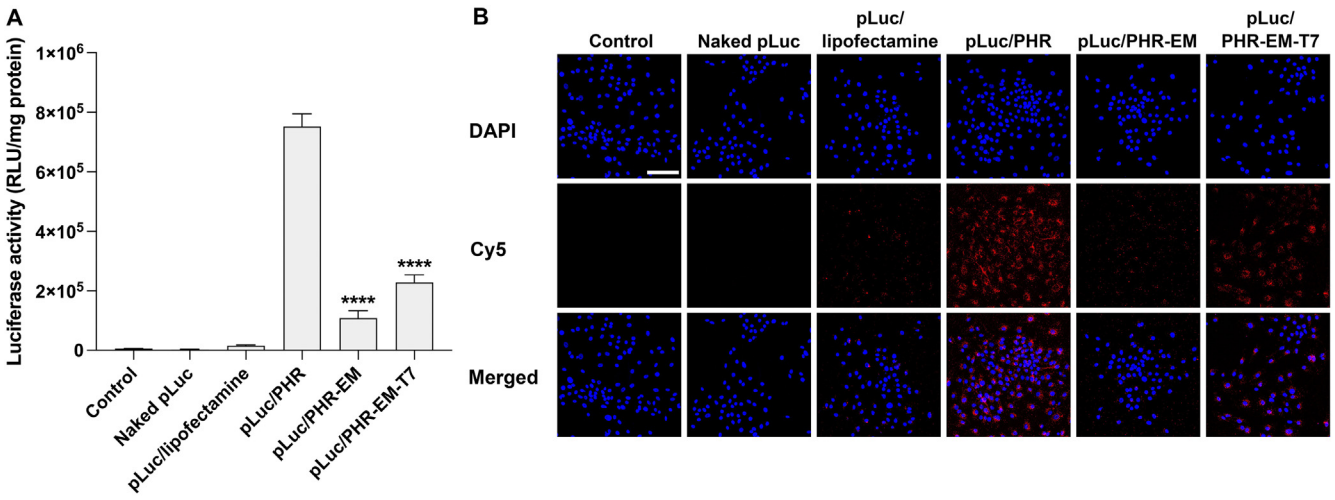

Fig. 4 – Transfection efficiencies of pLuc/PHR-EM and pLuc/PHR-EM-T7 in comparison to other carriers. (A) Luciferase assay. pLuc was transfected into C6 cells using lipofectamine, PHR, PHR-EM, or PHR-EM-T7 ($n = 4$). **** $P < 0.0001$ compared with the other samples. (B) Confocal microscopy study. The complexes were prepared with Cy5-pHSVtk. After transfection, the cellular uptake of pDNA was analyzed by confocal microscopy. The scale bar is 100 μm. (For interpretation of the references to colour in this figure legend, the reader is referred to the web version of this article.)

hydrophobic interaction, T7c, a cholesterol-conjugated T7 peptide, was used as referenced in a previous study [41]. Various amounts of T7c were mixed with the pDNA/PHR-EM complex, and the mixtures were subjected to extrusion. Then, pLuc/PHR-EM-T7 was transfected into C6 cells. The luciferase assay showed that pLuc/PHR-EM-T7 had higher transfection efficiency than pDNA/PHR-EM (Fig. 2C). The optimum ratio of T7c and the pLuc/PHR-EM complex with the highest transfection efficiency was 1:2 (pDNA:T7c) (Fig. 2C). At this ratio, the T7c integration rate to pDNA/PHR-EM was measured by precipitation of the complex with F648-pDNA. The results showed that the integration rate of T7c was 59.4% ± 1.9%.

Physical characterization was performed with the pDNA/PHR-EM and pDNA/PHR-EM-T7 complexes. TEM analysis indicated that the pHSVtk/PHR complex had a spherical shape (Fig. 3A). The pHSVtk/PHR-EM and pHSVtk/PHR-EM-T7 complexes were larger than the pHSVtk/PHR complex. The surface charge of pDNA/PHR was positive at approximately 30 mV (Fig. 3B). However, extrusion with pDNA/PHR and EM reduced the surface charge to −5 mV, suggesting that excessive positive charge of the pDNA/PHR complex was masked by EM (Fig. 3B). The negative charges of the complexes may be beneficial for systemic delivery, since the interactions with negatively charged serum proteins may be minimized and opsonization may have decreased. The complex size was also measured using dynamic light scattering. The size of pDNA/PHR was around 131.6 ± 2.1 nm (Fig. 3C). The sizes of the complexes were increased by the addition of EM, which agreed with the results of TEM. The sizes of pDNA/PHR-EM and pDNA/PHR-EM-T7 were 284.6 ± 3.4 nm and 281.9 ± 21.4 nm, respectively (Fig. 3C). The time-dependent size changes of pDNA/PHR-EM-T7 were also evaluated by dynamic light scattering. The results indicated that the size was not increased up to 1 h after complex preparation (Fig. 3D). After 1 h, the complex sizes increased along with time, suggesting that the complex might form aggregates.

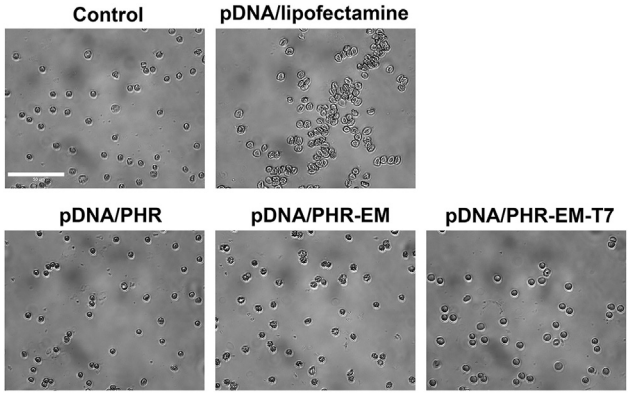

Fig. 5 – Hemocompatibility study. The pDNA/carrier complexes were incubated with erythrocytes. The samples were observed with a light microscope at 400× magnification.

3.2. *Comparison of pDNA/PHR-EM-T7 with other carriers*

The transfection efficiency values of pLuc/PHR-EM and pLuc/PHR-EM-T7 were compared with that of the pLuc/PHR or pLuc/lipofectamine complexes at their optimal weight ratios (Fig. 4A). PHR had a higher transfection efficiency than lipofectamine to C6 cells. This result was coincident with a previous study on PHR [29]. Transfection efficiencies of pLuc/PHR-EM and pLuc/PHR-EM-T7 were lower than that of pLuc/PHR (Fig. 4A), possibly due to their negative surface charge. Unlike the complexes, pLuc/PHR had a positive surface charge (Fig. 3B) and might interact with the negatively charged cell membrane more easily. This interaction might

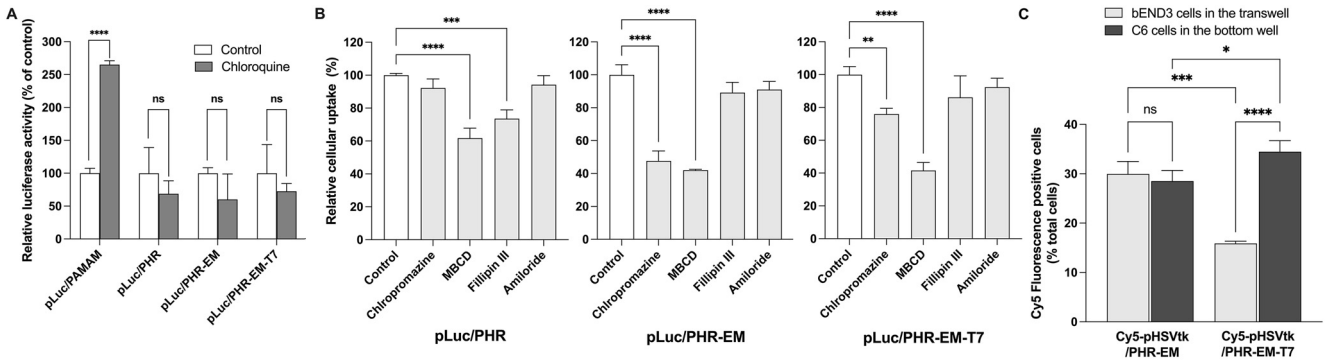

Fig. 6 – Effects of endocytosis inhibitors and transcytosis assay. (A) Effect of chloroquine on the transfection efficiency ($n = 4$). The complexes were transfected into C6 cells with or without chloroquine. (B) Effects of endocytosis inhibitors on cellular uptake($n = 4$). The complexes were transfected into C6 cells that were pre-treated with chlorpromazine, fillipin III, MβCD, and amiloride for 30 min. The cellular uptake was measured using flow cytometry. (C) Transcytosis assay ($n = 4$). Cy5-pHSVtk uptake was measured in bEND.3 brain endothelial cells and C6 cells. Cy5-pHSVtk/PHR/EM and Cy5-pHSVtk/PHR/EM-T7 were prepared and added to bEND.3 cells in transwells. Cellular uptakes of bEND.3 cells in the transwell and C6 cells in the bottom wells were measured with flow cytometry. * $P < 0.05$, ** $P < 0.01$, *** $P < 0.001$, and **** $P < 0.0001$. (For interpretation of the references to colour in this figure legend, the reader is referred to the web version of this article.)

increase the transfection efficiency of PHR compared with PHR-EM and PHR-EM-T7. However, this result does not indicate that the PHR-EM hybrid complex is ineffective for gene delivery. Positively charged pDNA/polymer complexes are more effective than negatively charged ones *in vitro* transfection due to their enhanced interactions with cellular membranes. However, biodistribution and toxicity results *in vivo* animal models suggest different results [42]. The positively charged particles can be easily cleared from the blood by opsonization. In addition, various factors such as liver toxicity, immune response, and hemocompatibility indicated that positively charged particles induce *in vivo* toxicity. This suggests that a certain decrease in transfection efficiency *in vitro* transfection does not indicate the reduction of gene delivery efficiency *in vivo*.

The transfection efficiency of pLuc/PHR-EM-T7 was higher than that of pLuc/PHR-EM Fig. 4A. This suggests that T7 on the surface of the complex increased the transfection efficiency into C6 glioblastoma cells. Since it was previously reported that C6 cells express a high level of transferrin receptors [20], the T7 peptide of pLuc/PHR-EM-T7 might bind to the receptors and increase the cellular uptake. Confocal microscopy also showed that the cellular uptake of Cy5-pLuc by pLuc/PHR-EM-T7 was higher than that of pLuc/PHR-EM, confirming that T7-peptide on pLuc/PHR-EM-T7 may facilitate the uptake of Cy5-pLuc into the cells (Fig. 4B). Also, as observed in Fig. 4A, the cellular uptake of Cy5-pLuc was detected at the highest level in the pLuc/PHR group (Fig. 4B).

A hemocompatibility study was carried out to evaluate the toxicity of the carrier in serum. The pDNA/carrier complexes were incubated with RBCs. As a result, the pLuc/lipofectamine complex induced aggregation of RBCs (Fig. 5). However, the pLuc/PHR, pLuc/PHR-EM, and pLuc/PHR-EM-T7 complexes did not induce aggregation of erythrocytes (Fig. 5). These confirmed the observation of the previous study, in which the pLuc/PHR complex had significantly lower toxicity compared with pLuc/lipofectamine and pLuc/PEI25k complexes. In addition, formation of a PHR-EM hybrid-complex did not induce any remarkable toxicity to erythrocytes compared with pLuc/PHR.

To evaluate endosomal escape ability, the cells were treated with chloroquine prior to transfection. Chloroquine is a widely used endosome destabilizing agent that can increase transfection efficiency if endosomal escape of the pDNA/carrier complex is not complete. Transfection efficiency of PHR was not enhanced by addition of chloroquine, suggesting that PHR can facilitate endosomal escape effectively without chloroquine. However, the transfection efficiency of PAMAM was greatly increased by treatment with chloroquine (Fig. 6A). This difference may be due to the proton sponge effect of histidine in PHR. The pDNA/PHR-EM and pDNA/PHR-EM-T7 complexes did not increase the transfection efficiency with chloroquine compared with the complexes without chloroquine (Fig. 6A). Therefore, it is likely that histidine moieties on PHRs may contribute to efficient endosomal escape in the pDNA/PHR, pDNA/PHR-EM, and pDNA/PHR-EM-T7. The results suggest that the pLuc/PHR, pLuc/PHR-EM, pLuc/PHR-EM-T7 complexes have endosomolytic ability, which may be due to the proton sponge effect of histidine moieties. In contrast, the transfection efficiencies of pDNA/PHR, pDNA/PHR-EM, and pDNA/PHR-EM-T7 complexes seemed to decrease slightly in the presence of chloroquine, although the difference was not statistically significant (Fig. 6A). This tendency may be due to the toxicity of chloroquine, reducing the viability of the transfected cells.

The cellular uptake pathway of complexes was analyzed by flow cytometry (Fig. 6B). Similar to a previous study [29], PHR was affected by methyl-β-cyclodextrin (MβCD). Since MβCD removes cholesterol from the cell membrane, the decrease of transfection efficiency suggests that PHR-mediated transfection may induce cholesterol-raft-dependent endocytosis. On the other hand, transfection efficiencies of pDNA/PHR-EM and pDNA/PHR-EM-T7 were reduced both by MβCD and by chlorpromazine (Fig. 6B).

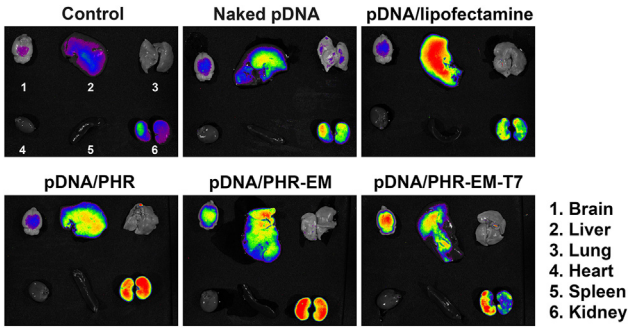

Fig. 7 – Biodistribution of pDNA/PHR-EM-T7 after systemic administration in the glioblastoma animal model. Naked Cy5.5-pHSVtk, Cy5.5-pHSVtk/lipofectamine, Cy5.5-pHSVtk/PHR, Cy5.5-pHSVtk/PHR-EM, and Cy5.5-pHSVtk/PHR-EM-T7 were prepared at their optimal ratios. The complexes were injected intravenously into the orthotopic glioblastoma animal model at 30 μg of Cy5.5-pHSVtk per rat. After 2 h, ex vivo fluorescence images were obtained using a Fluorescence In Vivo Imaging System.

Chlorpromazine inhibits clathrin-mediated endocytosis by translocating clathrin protein to intracellular vesicles [43,44]. These results indicate that clathrin-mediated endocytosis of the complexes may partly contribute to the entry of pDNA/PHR-EM and pDNA/PHR-EM-T7 into the cell. These effects may be partly due to EM, since exosomes enter cells by clathrin-mediated endocytosis.

To verify the transcytosis ability of pDNA/PHR-EM-T7, transwell experiments were performed with Cy5-pHSVtk/PHR-EM and Cy5-pHSVtk/PHR-EM-T7. bEND.3 mouse endothelial cells were seeded on the apical side of the transwell and cultured for production of endothelial layer. C6 cells were cultured on the bottom wells. Cy5-pHSVtk/PHR-EM and Cy5-pHSVtk/PHR-EM-T7 were added to the bEND.3 cells in the transwell. After 24 h, the cells in the transwell and bottom well were analyzed by flow cytometry. The results showed that the fluorescence signals in C6 cells were increased in the Cy5-pHSVtk/PHR-EM-T7 group, compared with the Cy5-pHSVtk/PHR/EM group (Fig. 6C). In addition, the fluorescence level in the bEND.3 cells of the Cy5-pHSVtk/PHR-EM-T7 group was lower than that of the Cy5-pHSVtk/PHR-EM group (Fig. 6C). The results suggest that the transcytosis process was facilitated by T7 decoration.

3.3. In vivo *biodistribution and liver toxicity in a glioblastoma animal model*

In vivo pDNA delivery was evaluated in the glioblastoma animals by intravenous injection. Cy5.5-pHSVtk was complexed with lipofectamine, PHR, PHR-EM, and PHR-EM-T7. After 2 h of injection, *ex vivo* fluorescence was investigated in an image box to evaluate biodistribution. Most of the Cy5.5-pHSVtk/lipofectamine complexes were taken up by the liver (Fig. 7). This result suggests that positively-charged pHSVtk/lipofectamine complexes were taken up by Kupffer cells [42,45]. In contrast, the pDNA/PHR, pDNA/PHR-EM, and pDNA/PHR-EM-T7 complexes accumulated more in the kidneys than the liver (Fig. 7). This showed that the complexes are more likely to be cleared rather than consumed in the liver. Fluorescence signals in the brain of the pDNA/PHR-EM group were higher than those in the pDNA/PHR group. This may be due to reduced clearance of pDNA/PHR-EM, allowing

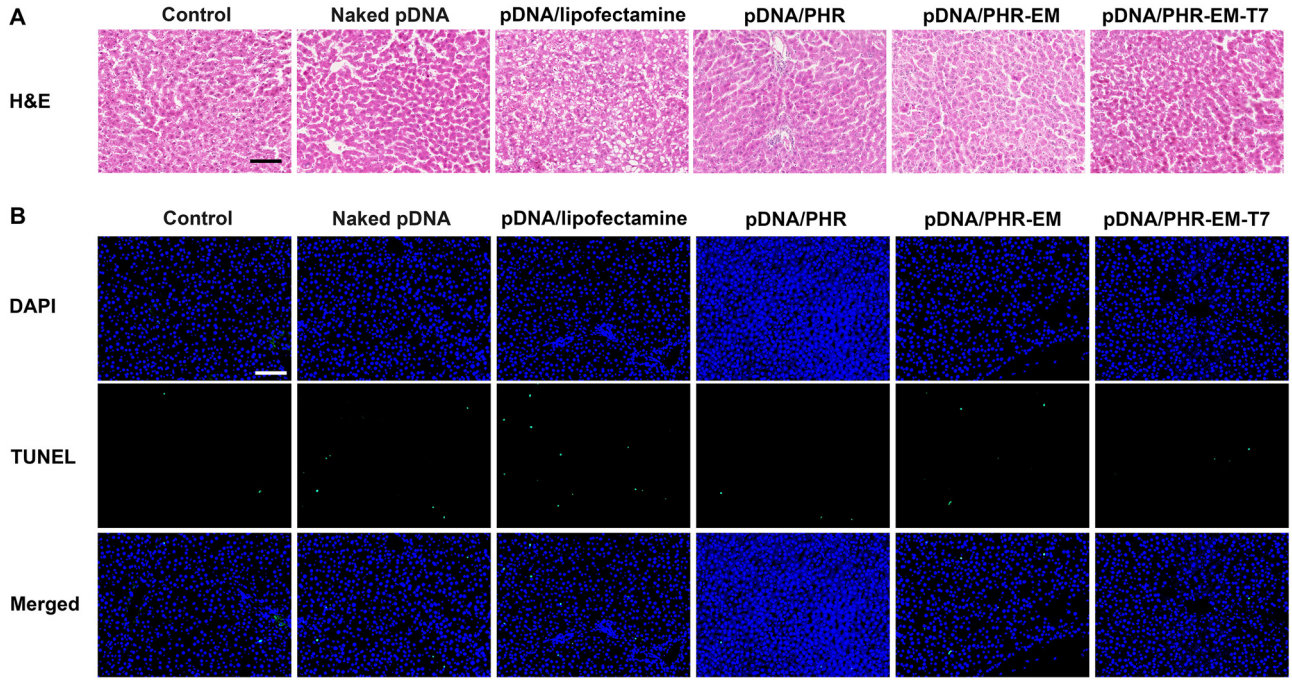

Fig. 8 – Liver toxicity of the pDNA/carrier complexes. The pHSVtk/carrier complexes were injected intravenously into the rat glioblastoma model. After 24 h, livers were subjected to H&E staining (A) and TUNEL assay (B). Scale bar: 200 μm.

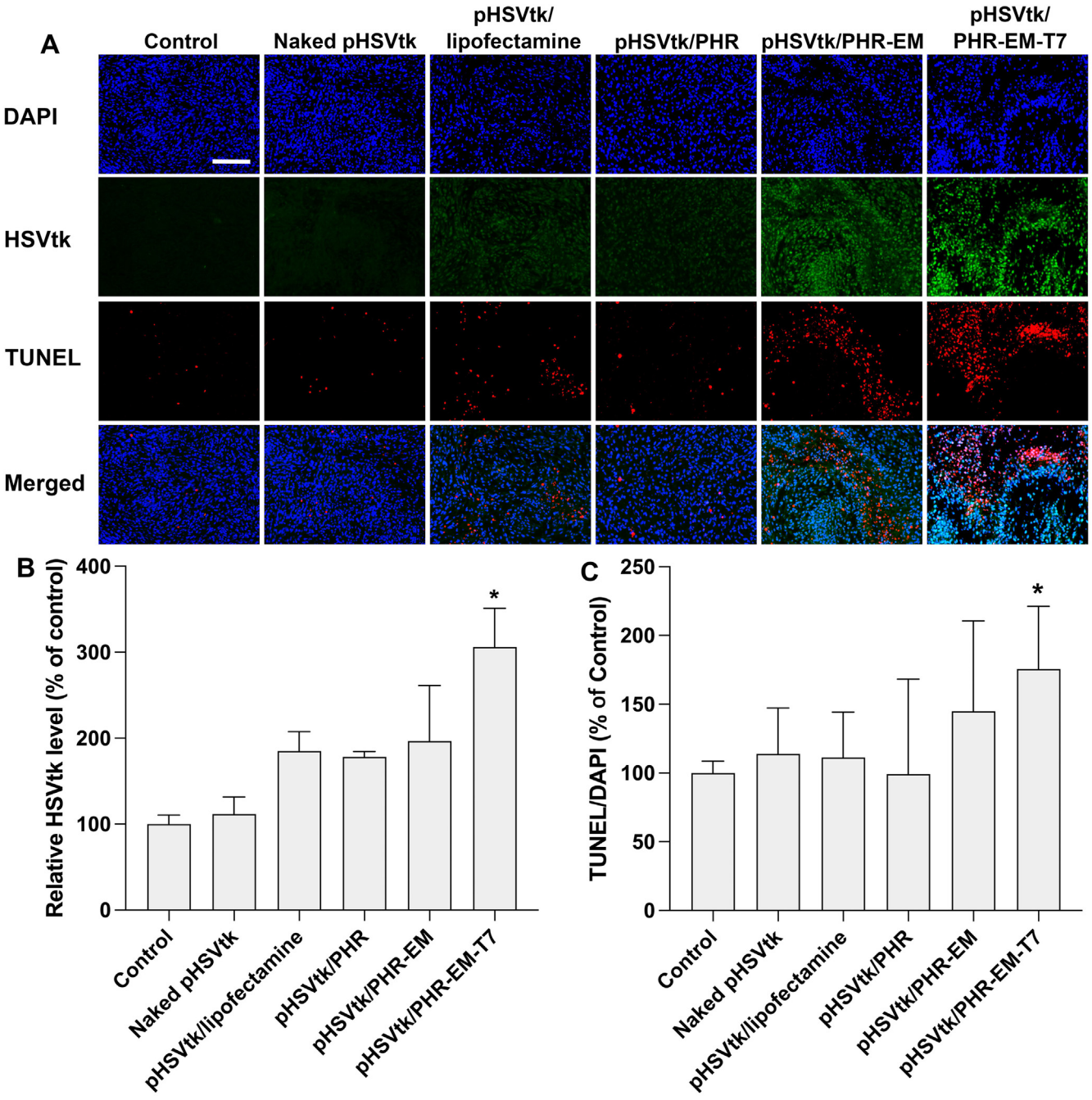

Fig. 9 – Expression of HSVtk and apoptosis, and tumor size. The pHSVtk/carrier complexes were injected intravenously into the rat glioblastoma model. After 24 h, the brains were harvested and subjected to (A) immunohistochemistry with anti-HSVtk antibody and TUNEL assay. (B) Quantitation of the HSVtk level ($n = 4$). *$P < 0.05$ compared with the other groups. (C) Quantification of the TUNEL signal ($n = 4$). *$P < 0.05$ compared with the control, pHSVtk/lipofectamine, and pHSVtk/PHR. (For interpretation of the references to colour in this figure legend, the reader is referred to the web version of this article.)

it a longer time to enter the brain. Another possibility is that EM from C6 cells may have a homotypic targeting effect, considering that cell-membranes from the cancer cells have targeting effects for the same types of cells [46]. pDNA/PHR-EM-T7 showed the highest fluorescence signals in the brain, confirming the effect of T7 peptides on transcytosis into the brain (Fig. 7). However, some of pDNA/PHR-EM-T7 complexes may accumulate in the endothelial cells in BBB or healthy cells in the brain. Therefore, we do not exclude the possibility that the complexes may induce cytotoxicity to healthy cells in the brain.

The H&E staining of the liver tissues was performed to evaluate the toxicity of the intravenous injection of the complexes (Fig. 8A). The pDNA/lipofectamine complexes in the liver induced damage, and this might be due to the positive charge of the pDNA/lipofectamine complex. This result agrees

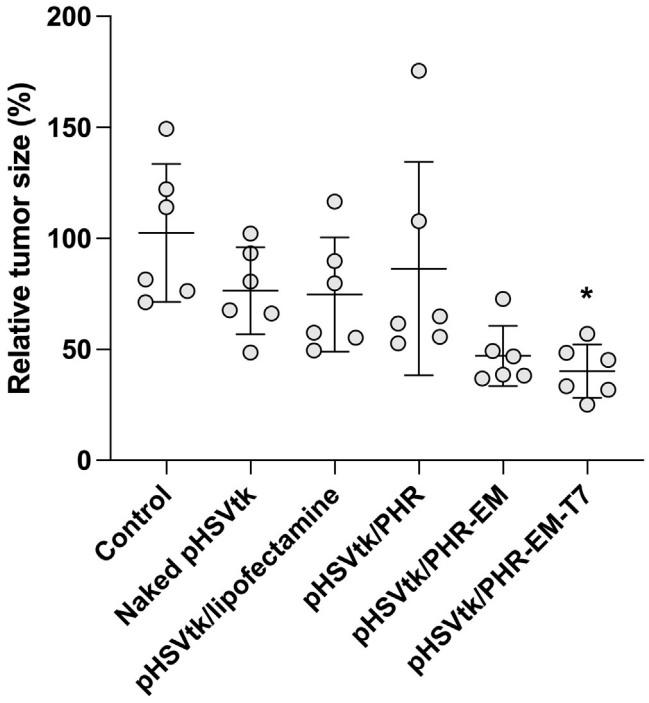

Fig. 10 – The pHSVtk/carrier complexes were injected intravenously into the rat glioblastoma model. After 24 h, the brains were harvested and subjected to Nissl staining. The tumor size is presented as percent of control ($n = 6$). * $P < 0.05$ compared with control and pHSVtk/PHR. (For interpretation of the references to colour in this figure legend, the reader is referred to the web version of this article.)

with the hemocompatibility assays (Fig. 5). Microsteatosis of hepatocytes was predominantly observed only two hours from injection. In contrast, there was no distinct damage in the pDNA/PHR group, but neutrophil infiltration was observed. These suggested that pDNA/PHR may induce immune responses in the liver, although cytotoxicity of PHR is relatively low. On the other hand, the pDNA/PHR-EM and pDNA/PHR-EM-T7 showed similar histochemical results to the control and naked groups (Fig. 8A). The apoptosis level in the liver tissues after intravenous injection of the complexes was measured by TUNEL assay. The number of apoptotic cells was not high in all the groups, but the apoptosis level was the highest in the pDNA/lipofectamine group (Fig. 8B). Overall results indicate that formation of a hybrid-complex with EM or EM-T7 may reduce cytotoxicity *in vivo*.

3.4. *Therapeutic effect of pHSVtk delivery in the orthotopic glioblastoma model*

pHSVtk/carrier complexes were injected intravenously into the orthotopic glioblastoma model. Seven days after injection, the rats were sacrificed, and the brains were analyzed. The gene expression and cell death caused by delivery of pHSVtk and GCV were observed by immunofluorescence staining with anti-HSVtk antibody and TUNEL assay (Fig. 9A). The results showed that HSVtk expression was induced by pHSVtk/PHR-EM and pHSVtk/PHR-EM-T7 compared with pHSVtk/lipofectamine and pHSVtk/PHR complexes (Fig. 9A and 9B). In particular, the HSVtk expression caused by pHSVtk/PHR-EM-T7 was higher than that by pHSVtk/PHR-EM, suggesting targeted delivery of the T7 peptide (Fig. 9A and 9B). Interestingly, as in Fig. 4, pDNA/PHR had higher transfection efficiency than pDNA/PHR-EM or pDNA/PHR-EM-T7 in the *in vitro* transfection assay. However, the tendency was different *in vivo* animal experiments. The enhanced delivery efficiency of EM-coated pDNA/EM complexes may be due to reduced interaction of blood components and opsonization, resulting in increase in circulation and delivery into the brain. In addition, T7 on the surface of the pDNA/PHR-EM complex might increase delivery efficiency of pDNA into the brain.

The TUNEL assay showed that the pHSVtk/PHR-EM complexes increased the apoptosis level compared with pHSVtk/lipofectamine and pHSVtk/PHR (Fig. 9A and 9C). However, apoptosis of the tumor cells was induced most effectively by pHSVtk/PHR-EM-T7 compared with the other complexes (Fig. 9A and 9C). This suggests that the delivery of pHSVtk by PHR-EM-T7 may induce gene expression, resulting in enhanced apoptosis.

Nissl staining was performed to evaluate tumor size (Fig. 10). The results showed that the pDNA/PHR-EM and pDNA/PHR-EM-T7 reduced the tumor size compared with the controls. Although there was no statistical difference, the tumor size in the pHSVtk/PHR-EM-T7 group was smaller than that in the pHSVtk/PHR-EM group. Therefore, HSVtk immunostaining, TUNEL assay, and Nissl staining indicated that the pHSVtk/pHR-EM-T7 hybrid-complex increased the delivery efficiency of pDNA into the brain. In Fig. 8A and 8B, HSVtk expression was induced by PHR-EM-T7, compared with PHR-EM. This result suggests that PHR-EM-T7 had higher delivery efficiency than PHR-EM. However, the apoptosis levels between pHSVtk/PHR-EM and pHSVtk/PHR-EM-T7 were not statistically different (Fig. 9C). In addition, the tumor sizes of pHSVtk/PHR-EM and pHSVtk/PHR-EM-T7 were not statistically different (Fig. 10). These results suggested that apoptosis was induced effectively by pHSVtk/PHR-EM in the glioblastoma animal model and therefore, further induction of apoptosis might not be significant, although pHSVtk/PHR-EM-T7 had higher delivery efficiency than pHSVtk/PHR-EM.

4. Conclusion

In this study, pDNA/PHR-EM-T7 was developed for systemic delivery of pDNA into a glioblastoma. pDNA/PHR-EM-T7 had an improved targeting delivery effect to glioblastoma after intravenous administration compared with pDNA/lipofectamine, pDNA/PHR, and pDNA/PHR-EM. In addition, therapeutic effects of pHSVtk/PHR-EM-T7 in the glioblastoma model were higher than those of pHSVtk/PHR and pHSVtk/lipofectamine. The enhanced tumor targeting is attributed to T7 peptide modification, which facilitates glioblastoma cell targeting and transcytosis through BBB. Based on all the data, enhanced targeting capability and therapeutic efficacy highlight potential of pDNA/PHR-EM-T7 as a promising approach for systemic pDNA delivery to glioblastoma.

For future applications, this platform technology could overcome the limitations of various carriers that face challenges in systemic delivery due to opsonization caused by positive charges. The method of attaching hydrophobic moieties, such as cholesterol, can be applied to other targeting peptides, making it feasible to use this approach for various tumors beyond glioblastoma. By utilizing different targeting peptides specific to other tumors, this technology can be adapted to a wide range of cancers, enhancing its versatility and potential impact in targeted cancer therapy.

Conflicts of interest

The authors declared no conflict of interest.

Acknowledgments

This work was supported by the Individual Basic Science & Engineering Research Program (NRF-2022R1A2B5B01001920) through the National Research Foundation, funded by the Ministry of Science and ICT in Korea.

Supplementary materials

Supplementary material associated with this article can be found, in the online version, at doi:10.1016/j.ajps.2024.101006.

References

[1] Adamson C, Kanu OO, Mehta AI, Di C, Lin N, Mattox AK, et al. Glioblastoma multiforme: a review of where we have been and where we are going. Expert Opin Investig Drugs 2009;18(8):1061–83.
[2] Gallego O. Nonsurgical treatment of recurrent glioblastoma. Curr Oncol 2015;22(4):E273–81.
[3] Hou LC, Veeravagu A, Hsu AR, Tse VC. Recurrent glioblastoma multiforme: a review of natural history and management options. Neurosurg Focus 2006;20(4):E5.
[4] Alemany R, Gomez-Manzano C, Balague C, Yung WK, Curiel DT, Kyritsis AP, et al. Gene therapy for gliomas: molecular targets, adenoviral vectors, and oncolytic adenoviruses. Exp Cell Res 1999;252(1):1–12.
[5] Castro MG, Candolfi M, Kroeger K, King GD, Curtin JF, Yagiz K, et al. Gene therapy and targeted toxins for glioma. Curr Gene ther 2011;11(3):155–80.
[6] Rainov NG. A phase III clinical evaluation of herpes simplex virus type 1 thymidine kinase and ganciclovir gene therapy as an adjuvant to surgical resection and radiation in adults with previously untreated glioblastoma multiforme. Hum Gene Ther 2000;11(17):2389–401.
[7] Han S, Lee Y, Lee M. Biomimetic cell membrane-coated DNA nanoparticles for gene delivery to glioblastoma. J Control Release 2021;338:22–32.
[8] Tamura R, Miyoshi H, Yoshida K, Okano H, Toda M. Recent progress in the research of suicide gene therapy for malignant glioma. Neurosurg Rev 2021;44(1):29–49.
[9] Mesnil M, Yamasaki H. Bystander effect in herpes simplex virus-thymidine kinase/ganciclovir cancer gene therapy: role of gap-junctional intercellular communication. Cancer Res 2000;60(15):3989–99.
[10] Kadry H, Noorani B, Cucullo L. A blood-brain barrier overview on structure, function, impairment, and biomarkers of integrity. Fluids Barriers CNS 2020;17(1):69.
[11] Alvarez-Erviti L, Seow YQ, Yin HF, Betts C, Lakhal S, Wood MJA. Delivery of siRNA to the mouse brain by systemic injection of targeted exosomes. Nat Biotech 2011;29(4):341–5.
[12] Kim M, Kim G, Hwang DW, Lee M. Delivery of high mobility group box-1 siRNA using brain-targeting exosomes for ischemic stroke therapy. J Biomed Nanotechnol 2019;15(12):2401–12.
[13] Kim M, Lee Y, Lee M. Hypoxia-specific anti-RAGE exosomes for nose-to-brain delivery of anti-miR-181a oligonucleotide in an ischemic stroke model. Nanoscale 2021;13(33): 14166–14178.
[14] Wu JY, Li YJ, Hu XB, Huang S, Luo S, Tang T, et al. Exosomes and biomimetic nanovesicles-mediated anti-glioblastoma therapy: a head-to-head comparison. J Control Release 2021;336:510–21.
[15] Lee Y, Kim M, Ha J, Lee M. Brain-targeted exosome-mimetic cell membrane nanovesicles with therapeutic oligonucleotides elicit anti-tumor effects in glioblastoma animal models. Bioeng Transl Med 2023;8(2):e10426.
[16] Ding Y, Wang Y, Hu Q. Recent advances in overcoming barriers to cell-based delivery systems for cancer immunotherapy. Exploration (Beijing) 2022;2(3):20210106.
[17] Kim S, Ullah I, Beloor J, Chung K, Kim J, Yi Y, et al. Systemic treatment with siRNA targeting gamma-secretase activating protein inhibits amyloid-beta accumulation in Alzheimer's disease. Biomater Res 2024;28:0027.
[18] Ruan S, Zhou Y, Jiang X, Gao H. Rethinking CRITID procedure of brain targeting drug delivery: circulation, blood brain barrier recognition, intracellular transport, diseased cell targeting, internalization, and drug release. Adv Sci 2021;8(9):2004025.
[19] Yang J, Li Y, Jiang S, Tian Y, Zhang M, Guo S, et al. Engineered brain-targeting exosome for reprogramming immunosuppressive microenvironment of glioblastoma. Exploration (Beijing) 2024:20240039.
[20] Kim G, Kim M, Lee Y, Byun JW, Hwang DW, Lee M. Systemic delivery of microRNA-21 antisense oligonucleotides to the brain using T7-peptide decorated exosomes. J Control Release 2020;317:273–81.
[21] Roerig J, Schulz-Siegmund M. Standardization approaches for extracellular vesicle loading with oligonucleotides and biologics. Small 2023;19(40):2301763.
[22] Ju Z, Ma J, Wang C, Yu J, Qiao Y, Hei F. Exosomes from iPSCs delivering siRNA attenuate intracellular adhesion molecule-1 expression and neutrophils adhesion in pulmonary microvascular endothelial cells. Inflammation 2017;40(2):486–96.
[23] Kooijmans SAA, Stremersch S, Braeckmans K, de Smedt SC, Hendrix A, Wood MJA, et al. Electroporation-induced siRNA precipitation obscures the efficiency of siRNA loading into extracellular vesicles. J Control Release 2013;172(1):229–38.
[24] McAndrews KM, Xiao F, Chronopoulos A, LeBleu VS, Kugeratski FG, Kalluri R. Exosome-mediated delivery of CRISPR/Cas9 for targeting of oncogenic Kras(G12D) in pancreatic cancer. Life Sci Alliance 2021;4(9):e202000875.
[25] Wallen M, Aqil F, Spencer W, Gupta RC. Exosomes as an emerging plasmid delivery vehicle for gene therapy. Pharmaceutics 2023;15(7):1832.
[26] Xia X, Shi B, Wang L, Liu Y, Zou Y, Zhou Y, et al. From mouse to mouse-ear cress: nanomaterials as vehicles in plant biotechnology. Exploration (Beijing) 2021;1(1):9–20.
[27] Ma J, Li N, Wang J, Liu Z, Han Y, Zeng Y. *In vivo* synergistic tumor therapies based on copper sulfide photothermal therapeutic nanoplatforms. Exploration (Beijing) 2023;3(5):20220161.

[28] Oh J, Kim SM, Lee EH, Kim M, Lee Y, Ko SH, et al. Messenger RNA/polymeric carrier nanoparticles for delivery of heme oxygenase-1 gene in the post-ischemic brain. Biomater Sci 2020;8(11):3063–71.
[29] Lee Y, Lee J, Kim M, Kim G, Choi JS, Lee M. Brain gene delivery using histidine and arginine-modified dendrimers for ischemic stroke therapy. J Control Release 2021;330:907–19.
[30] Bikram M, Lee M, Chang CW, Janat-Amsbury MM, Kern SE, Kim SW. Long-circulating DNA-complexed biodegradable multiblock copolymers for gene delivery: degradation profiles and evidence of dysopsonization. J Control Release 2005;103(1):221–33.
[31] Han LA, Huang RQ, Liu SH, Huang SX, Jiang C. Peptide-conjugated PAMAM for targeted doxorubicin delivery to transferrin receptor overexpressed tumors. Mol Pharm 2010;7(6):2156–65.
[32] Kim HA, Park JH, Yi N, Lee M. Delivery of hypoxia and glioma dual-specific suicide gene using dexamethasone conjugated polyethylenimine for glioblastoma-specific gene therapy. Mol Pharm 2014;11(3):938–50.
[33] Piao C, Zhuang C, Choi M, Ha J, Lee M. A RAGE-antagonist peptide potentiates polymeric micelle-mediated intracellular delivery of plasmid DNA for acute lung injury gene therapy. Nanoscale 2020;12(25):13606–17.
[34] Zhuang C, Piao C, Kang M, Oh J, Lee M. Hybrid nanoparticles with cell membrane and dexamethasone-conjugated polymer for gene delivery into the lungs as therapy for acute lung injury. Biomater Sci 2023;11(9):3354–64.
[35] Kim M, Oh J, Lee Y, Lee EH, Ko SH, Jeong JH, et al. Delivery of self-replicating messenger RNA into the brain for the treatment of ischemic stroke. J Control Release 2022;350(350):471–85.
[36] Jeong EJ, Lee J, Kim HS, Lee KY. *In vitro* cellular uptake and transfection of oligoarginine-conjugated glycol chitosan/siRNA nanoparticles. Polymers (Basel) 2021;13(23):4219.
[37] Lee JW, Kim HS, Yon SJ, Matsumoto T, Lee SK, Lee KY. *In vitro* culture of hematopoietic stem cell niche using angiopoietin-1-coupled alginate hydrogel. Int J Biol Macromol 2022;209(Pt B):1893–9.
[38] Ha J, Kim M, Lee Y, Lee M. Intranasal delivery of self-assembled nanoparticles of therapeutic peptides and antagomirs elicits anti-tumor effects in an intracranial glioblastoma model. Nanoscale 2021;13(35):14745–59.
[39] Park JH, Han J, Lee M. Thymidine kinase gene delivery using curcumin loaded peptide micelles as a combination therapy for glioblastoma. Pharm Res 2015;32(2):528–37.
[40] Chung S, Yi Y, Ullah I, Chung K, Park S, Lim J, et al. Systemic treatment with Fas-blocking peptide attenuates apoptosis in brain ischemia. Int J Mol Sci 2024;25(1).
[41] Lee Y, Kim M, Ha J, Lee M. Brain-targeted exosome-mimetic cell membrane nanovesicles with therapeutic oligonucleotides elicit anti-tumor effects in glioblastoma animal models. Bioeng Transl Med 2022;8(2):e10426.
[42] Xiao K, Li Y, Luo J, Lee JS, Xiao W, Gonik AM, et al. The effect of surface charge on *in vivo* biodistribution of PEG-oligocholic acid based micellar nanoparticles. Biomaterials 2011;32(13):3435–46.
[43] Sahay G, Alakhova DY, Kabanov AV. Endocytosis of nanomedicines. J Control Release 2010;145(3):182–95.
[44] El-Sayed A, Harashima H. Endocytosis of gene delivery vectors: from clathrin-dependent to lipid raft-mediated endocytosis. Mol Ther 2013;21(6):1118–30.
[45] Sun X, Wang G, Zhang H, Hu S, Liu X, Tang J, et al. The blood clearance kinetics and pathway of polymeric micelles in cancer drug delivery. ACS Nano 2018;12(6):6179–92.
[46] Lee H, Bae K, Baek AR, Kwon EB, Kim YH, Nam SW, et al. Glioblastoma-derived exosomes as nanopharmaceutics for improved glioma treatment. Pharmaceutics 2022;14(5):1002.